ACS APPLIED MATERIALS & INTERFACES

Forum Article

www.acsami.org

Statistical Length Measurement Method by Direct Imaging of Carbon Nanotubes

E. Amram Bengio,[†,‡] Dmitri E. Tsentalovich,[†] Natnael Behabtu,[†] Olga Kleinerman,[‡] Ellina Kesselman,[‡] Judith Schmidt,[‡] Yeshayahu Talmon,[‡] and Matteo Pasquali*[,†,§,∥]

[†]Department of Chemical and Biomolecular Engineering, The Smalley Institute for Nanoscale Science and Technology, Rice University, Houston, Texas 77005, United States

[‡]Department of Chemical Engineering, Technion-Israel Institute of Technology and The Russell Berrie Nanotechnology Institute (RBNI), Haifa 32000, Israel

[§]Department of Chemistry, Rice University, Houston, Texas 77005, United States

[∥]Department of Materials Science and NanoEngineering, Rice University, Houston, Texas 77005, United States

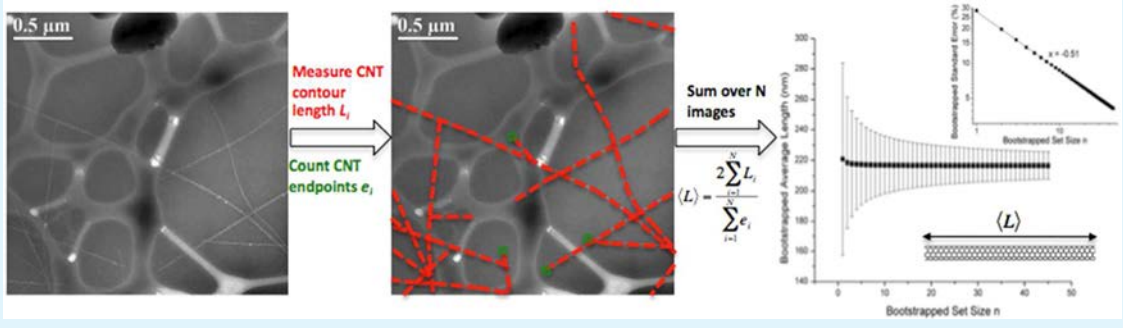

ABSTRACT: The influence of carbon nanotube (CNT) length on their macroscopic properties requires an accurate methodology for CNT length measurement. So far, existing techniques are limited to short (less than a few micrometers) CNTs and sample preparation methods that bias the measured values. Here, we show that the average length of carbon nanotubes (CNTs) can be measured by cryogenic transmission electron microscopy (cryo-TEM) of CNTs in chlorosulfonic acid. The method consists of dissolving at low concentration CNTs in chlorosulfonic acid (a true solvent), imaging the individual CNTs by cryo-TEM, and processing and analyzing the images to determine CNT length. By measuring the total CNT contour length and number of CNT ends in each image, and by applying statistical analysis, we extend the method to cases where each CNT is long enough to span many cryo-TEM images, making the direct length measurement of an entire CNT impractical. Hence, this new technique can be used effectively to estimate samples in a wide range of CNT lengths, although we find that cryo-TEM imaging may bias the measurement towards longer CNTs, which are easier to detect. Our statistical method is also applied to AFM images of CNTs to show that, by using only a few AFM images, it yields estimates that are consistent with literature techniques, based on individually measuring a higher number of CNTs.

KEYWORDS: *carbon nanotubes, chlorosulfonic acid, length measurement, cryo-TEM, bootstrap method, statistical re-sampling*

INTRODUCTION

Carbon nanotubes (CNTs) are tubular molecules of graphitic carbon with diameters on the order of 1 nm to several nanometers, and lengths typically ranging from several hundred nanometers to tens of micrometers, although CNTs with lengths of up to several millimeters have also been grown.[1] CNTs have excellent mechanical,[2] thermal,[3] and electrical[4] properties, and this unique combination holds great promise for a wide variety of applications.[5] However, the macroscopic properties of CNT materials are typically several orders of magnitude lower than those of individual CNTs. This has been attributed to the many difficulties inherent to processing raw CNT material into a usable form for a specific application,[6] particularly because of its lack of solubility in almost all liquids.[7] Previous work has shown that CNTs form true solutions in chlorosulfonic acid,[8,9] which is the best solvent in the family of CNT acid solvents,[8,10−12] allowing for the spinning of macroscopic fibers[9,13] and coating of films[14] from these solutions. Theoretical calculations[15] and experimental results[16] have shown that the tensile strength of a CNT fiber scales linearly with the average aspect ratio of the individual constituent CNTs; similar considerations can be made on electrical and thermal conductivity. Similarly, CNT length

Special Issue: Applications of Hierarchical Polymer Materials from Nano to Macro

Received: January 21, 2014
Accepted: April 4, 2014
Published: April 28, 2014

   dx.doi.org/10.1021/am500424u | *ACS Appl. Mater. Interfaces* 2014, 6, 6139−6146

affects the properties of CNT films. Therefore, it is important to accurately characterize CNTs length, to assess the potential of as-produced CNTs to yield materials with desirable macroscale properties.

Many techniques have been reported to measure average CNT length; they all face significant drawbacks, particularly when applied to long CNTs.[17] A common imaging technique involves the use of atomic force microscopy (AFM) on CNT dispersions.[18,19] However, AFM sample preparation for these systems always involves sonication; moreover, the differential suspension stability of long CNTs can bias CNT deposition onto the imaging substrate. Moreover, AFM length estimates rely on individually measuring a large number of CNTs to obtain statistically meaningful averages, which is time-intensive, in terms of sample preparation and analysis. Similarly, the length of CNTs has been measured by dynamic light scattering (DLS), which also requires sample sonication. Several studies have shown that sonication breaks CNTs, reducing their average length, and therefore introducing a measurement bias.[20−23] Scanning electron microscopy (SEM) has also been reported to measure the lengths of aligned, carpet-grown CNTs, but the method assumes that all CNTs have the same length and that the height of the carpet is an accurate estimate of such length. However, studies have shown that chemical vapor deposition (CVD)-grown CNT carpets have different densities along the height of the carpet, with the implication that CNTs do not grow continuously from the substrate all the way to the top of the carpet.[24] Characterization of CNT length distribution has also been achieved through the use of shear-aligned photoluminescence[25] and shear rheology in dilute suspensions or solutions.[26] However, shear rheometers cannot measure the zero-shear viscosity of suspensions of dilute CNTs longer than ∼1 μm (because of shear-induced alignment). Recent work by Zheng and co-workers[27] has shown that length fractionation of CNT populations with standard deviations of 30%−40% is achievable via selective clustering of CNT dispersions in DNA.

Here, we present a new method for measuring CNT length over a wide range of lengths. By using our earlier methodology,[28,29] we dissolve CNTs in chlorosulfonic acid and image them via cryo-TEM. The use of a true solvent eliminates the sonication-related problems faced by other imaging methods such as AFM or DLS. To avoid limitations in CNT length due to the limited size of high-magnification cryogenic transmission electron microscopy (cryo-TEM) images (∼1−2 μm), we use total imaged contour length and number of ends to extract the CNT average length. Because direct imaging is time-intensive, we apply a statistical method that allows us to estimate the average CNT length from relatively few images. This method also yields an estimate of how additional images change the running length estimate, providing a cutoff in the number of images sufficient for statistically significant measurement of CNT length. The usefulness of the statistical method is demonstrated on both cryo-TEM images as well as AFM images of CNTs.

EXPERIMENTAL METHODS

Several different samples of single-walled carbon nanotubes (SWNTs) and multiwalled carbon nanotubes (MWNTs) were measured in this study; they include high-pressure carbon monoxide (HiPco) SWNTs produced at Rice University,[30] CVD CNTs produced at Rice University,[31] a mixture of single-, double-, and triple-walled CNTs produced by Continental Carbon Nanotechnologies, Inc. (CCNI, Houston, TX), and laser vaporization SWNTs from biological char ("biolaser"), produced by the National Research Council of Canada.[33−35] The biolaser SWNTs were used both in raw form or purified with sulfuric acid to remove residual nongraphitic carbon.

The starting CNT material was dissolved in chlorosulfonic acid (CSA) at 5−100 ppm wt. Sample preparation was carried out in a glove box continuously purged with dry air, and all vials were sealed with Teflon tape. To ensure homogeneous CNT concentration, the solutions were mixed with a stir-bar for 12 h. Cryo-specimens were prepared inside a controlled environment vitrification system (CEVS)[36] at 25 °C with continuous purging of nitrogen gas, preventing acid contact with moisture. A small amount (ca. 3 μL) of solution was deposited onto a transmission electron microscopy (TEM) grid consisting of holey carbon and copper. The sample was rapidly vitrified in liquid nitrogen and then transferred to a pre-cooled TEM system. Specimens were examined in a FEI Tecnai 12 G^2 TEM system at an accelerating voltage of 120 kV. A Gatan 626 cryo-specimen holder was used to maintain the vitrified specimens below −175 °C. Specimens were studied in the low-dose imaging mode to minimize electron beam exposure and radiation damage.

Images were recorded digitally by a high-resolution 2k × 2k Gatan US1000 cooled CCD camera using the Digital Micrograph software (Gatan, U.K.). Images were pre-processed with Digital Micrograph, and a post-processing step involving the use of various noise-reducing filters in MATLAB was also carried out, when needed. Measurements of CNT length in cryo-TEM images were carried out using the Measuring Tool in Adobe Photoshop (CS4), and CNT end points were counted visually.

AFM samples were prepared and imaged according to the methods reported in ref 37. For AFM images, a MATLAB code was written to detect individual CNTs and their end points, based on three user-adjusted parameters, similar to the method reported in ref 38, but by measuring total CNT contour length rather than the length of each individual CNT. The first parameter controlled the sensitivity of the thresholding to convert the image from grayscale intensity to a binary image. The second parameter defined a minimum eccentricity, i.e., the ratio of the distance between the foci of the ellipse and the length of its major axis; objects that were not eccentric enough to be considered CNTs were discarded from the analysis. Finally, the third parameter defined a maximum average height value above which an object was considered to correspond to a bundle of CNTs and was discarded to avoid undercounting CNT end points that might not be visible in the bundle. The parameters were adjusted until satisfactory visual confirmation of the CNT and CNT end point detection was achieved, by overlapping the detection result with the original AFM image.

STATISTICAL METHODS: THE BOOTSTRAP

A typical dataset consists of a number of images N taken for a specific sample of CNTs. Each image i is associated with two measured variables: l_i and e_i, where l_i is the total CNT contour length measured in image i and e_i is the total number of CNT end points detected in image i. Defining A_i as the area of each image, n_t the total number of CNTs, and $\langle L \rangle$ the average CNT length, the density of ends (ρ_e) and the contour length density (ρ_l) are

$$\rho_e = \frac{\sum e_i}{\sum A_i} = \frac{2n_t}{Nw^2} \quad (1)$$

$$\rho_l = \frac{\sum l_i}{\sum A_i} = \frac{n_t \langle L \rangle}{Nw^2} \quad (2)$$

where $A_i = w^2$ in the case of identical square images (as in our cryo-TEM). Combining eqs 1 and 2 gives

$$\langle L \rangle = \frac{2n_t \langle L \rangle}{Nw^2} \frac{Nw^2}{2n_t} = 2\frac{\rho_e}{\rho_l} \quad (3)$$

or, equivalently, in terms of directly measured quantities,

$$\langle L \rangle = 2\frac{\sum_{i=1}^{N} l_i}{\sum_{i=1}^{N} e_i} \tag{4}$$

To compute a value for the standard error of this estimate, we use the "bootstrap" method.[39] The bootstrap method relies on the assumption that any dataset parameter (such as mean length, length variance) is an unbiased estimate (in the statistical sense) of the true value of this parameter, i.e., that the estimator converges to the true value of the parameter in the limit of infinite sample size. Thus, the bootstrap method can be used only if the estimates of average CNT length and variance in CNT length in the dataset are unbiased estimates for the true values of these parameters. In the context of our method, this assumption means that the total CNT contour length and total number of ends counted in our images are only a function of the CNT population's true average length and variance. If the CNT dispersion is of poor quality, or there is a preferential CNT orientation, then the resulting fluctuations in CNT end point and length density across images may induce an additional variance that is unrelated to the CNT population's true variance. The concentration of CNTs in the solutions was chosen so that the solution was isotropic, i.e., below the cloud point of the isotropic phase (where the nematic phase first appears); the cloud point was calculated based on the theory given in ref 40. The cryo-TEM images show that the CNTs in our samples are indeed randomly oriented; thus, eq 4 provides us with an unbiased estimate of average CNT length, since there is no bias in either e_i or l_i.

Datasets that contain no CNT end points are problematic, because they yield infinite estimates for $\langle L \rangle$ through eq 4. We denote the number of images containing zero CNT end points by N_p. Because the bootstrap method involves picking n images from the complete dataset with replacement (once picked, an image is not removed from the set and therefore can be picked more than once), then the probability of selecting n images containing zero CNT end points is

$$P\left(\sum_{i=1}^{n} e_i = 0\right) = \frac{{N_p}^n}{N^n} = \left(\frac{N_p}{N}\right)^n \tag{5}$$

Equation 5 shows that, as long as $N > N_p$ and the size n of our bootstrapped set is sufficiently large, the probability of selecting a set that would yield an infinite estimate for L is negligible. Therefore, neglecting these sets for our bootstrapped sets would not induce any significant statistical bias. Equivalently, the dataset must satisfy the condition

$$\left(\frac{N_p}{N}\right)^n \ll 1 \tag{6}$$

Of course, as the CNT length grows, the fraction of images with no ends increases accordingly, and the size n of the bootstrap set must be enlarged for the method to work. When this condition is met, then, within the limit of large N_{boot}, the bootstrap average $\langle L_{boot} \rangle$ converges to $\langle L \rangle$ and can be used as the unbiased estimate of the CNT average length:

$$\langle L \rangle \approx \langle L_{boot} \rangle = \frac{1}{N_{boot}} \sum_{b=1}^{N_{boot}} \langle L_b \rangle = \frac{2}{N_{boot}} \sum_{b=1}^{N_{boot}} \sum_{i=1}^{n} \frac{l_{i,b}}{e_{i,b}} \tag{7}$$

Here, the index b denotes the bth bootstrapped set. The error in this estimate is then approximately equal to the standard deviation σ_b of the bootstrapped sets:[39]

$$se_{\langle L \rangle} = \sqrt{\frac{N}{N-1}}\,\sigma_b \approx \sigma_b \tag{8}$$

In addition, while it is conventional to choose $n = N$ for bootstrap analysis (to maximize sample size), graphical visualization of the bootstrap standard errors as a function of n is useful to determine whether the error reaches an expected asymptotic behavior as n approaches N. If such asymptote is not approached, more images should be acquired and analyzed before a maximally accurate estimate of $\langle L \rangle$ is obtained. The standard error is plotted as a function of n and fitted to a power-law of the form

$$se_{\langle L \rangle} = kn^x \tag{9}$$

If the bootstrapped standard error is a true estimate for the sample variance, then, from classical statistics, it should depend on the inverse square root of the sample size, i.e., $x \approx -0.5$.

RESULTS AND DISCUSSION

Cryo-TEM Imaging. Figure 1 shows a typical cryo-TEM image. Long, individual CNTs are clearly visible, partially due to selective sample irradiation damage at doses of 100 e/Å^2, which produce the small white "bubbles" along the CNTs.[41] Figure 1 shows that the pristine CNTs in chlorosulfonic acid are clearly distinguishable. However, as CNT length grows and CNTs span multiple images, the imaging process struggles to follow each individual CNT continuously, because of the increased probability that some portion of the CNT may be hidden by crystallized acid, impurities, thicker sample areas, or by the holey carbon film. As CNT length increases, so does the likelihood that the CNT might extend into a portion of the sample film that cannot be imaged because of its thickness, the presence of artifacts, or any other number of imaging issues.

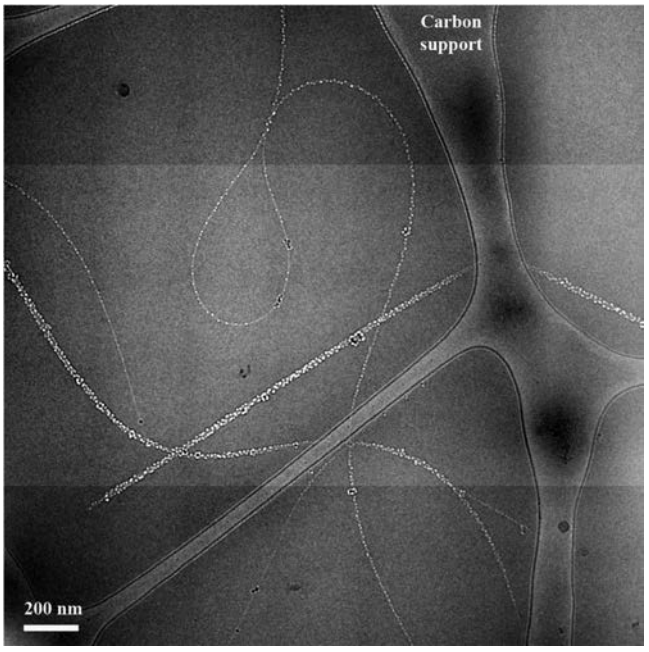

Figure 1. Cryo-TEM micrograph of CCNI 1101 CNTs dissolved in HSO_3Cl at 20 ppm wt.

Figure 2 shows a collage of three micrographs in an attempt to follow a long CNT. However, near the edges of the collage, the

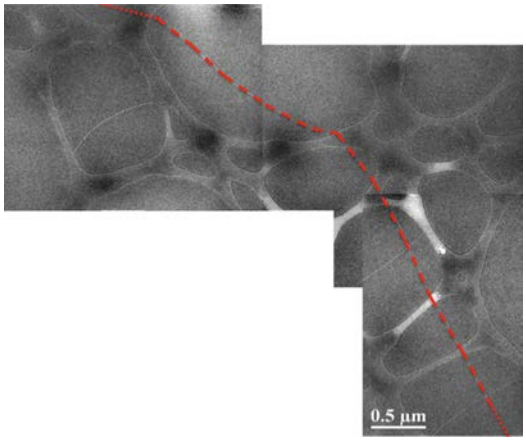

Figure 2. Montage of cryo-TEM micrograph of CCNI 1101 CNTs dissolved in HSO_3Cl at 20 ppm wt. A single, long (>5 μm) CNT can be traced across three frames (long red dashed line); however, because of experimental limitations (low contrast in portions of the sample that are too thick), the remainder of the CNT cannot be traced or measured with certainty (short red dashed lines).

sample was too thick to allow further imaging of the tube. This exemplifies how the high aspect ratio of these molecules can induce a persistent experimental bias in favor of shorter length estimates, because of the difficulties inherent in fully imaging a single, long CNT.

We circumvent these difficulties by measuring the total contour length and number of end points, as outlined in the derivation of eq 4. Briefly, we image various parts of each sample without attempting to follow any individual CNT, producing the initial dataset of N images. Figure 3 shows typical images for the six samples studied in this work. We then manually measured the total CNT length, and counted the number of CNT end points found in each image. A typical micrograph and length measurement result are shown in Figure 4. CNT contour length was measured only if it was in an area of the micrograph with sufficiently high contrast such that one also would be able to conclusively determine any potential end points. CNTs straddling the holey carbon film were included if they clearly continued through the film sections (see green arrows in Figure 4). Regardless of whether branching points were present (as shown in Figure 4) giving evidence that some of the CNTs were indistinguishably bundled together, no portion of any CNT was measured more than once. The justification behind this method is that bundles are rare in these very dilute suspensions in a true solvent. Thus, even though some CNTs are bundled together, the corresponding CNT length is still included in the measurement.

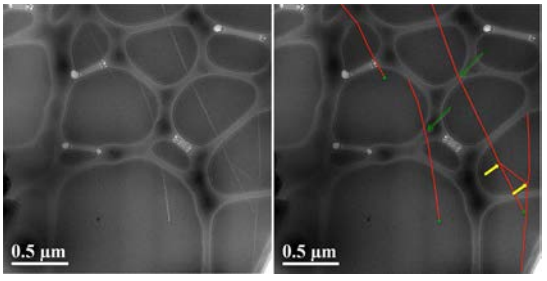

Figure 4. (left) Cryo-TEM micrograph of CCNI 1101 CNTs dissolved in HSO_3Cl at 20 ppm wt. and (right) overlapping manual length measurement result showing the measured CNT length in red and counted CNT end points with green plus sign (+) symbols. The yellow arrows indicate branching points. The green arrows indicate portions of CNTs that are still visible whilst straddling the holey carbon film.

Statistical Analysis. The results of the statistical analysis of all cryo-TEM datasets are shown in Table 1. Based on the values of N, N_p, and n in Table 1, all our datasets satisfy the condition specified by eq 6.

Because N_{boot} is large, a strong dependence of $\langle L_{boot} \rangle$ on n is not expected, unless the omission of zero-end point bootstrapped sets were to have an influence on the estimate, i.e., if

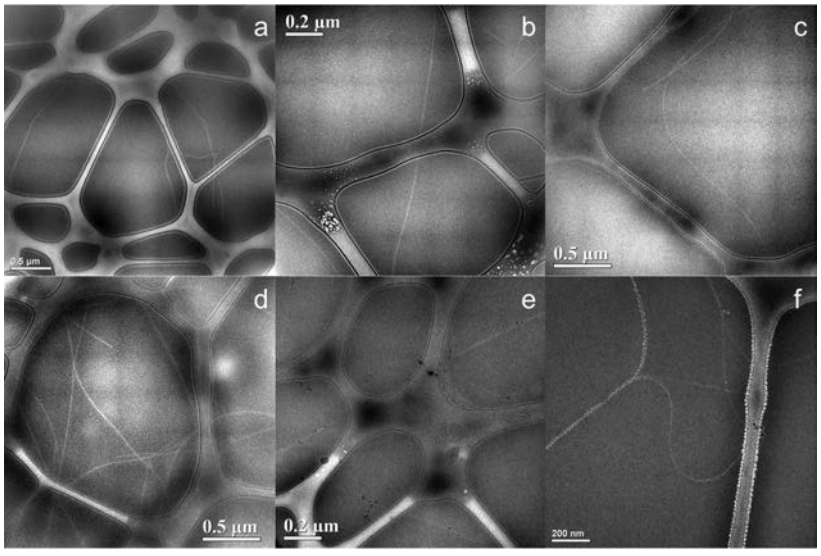

Figure 3. Cryo-TEM micrograph of different CNT batches dispersed at various weight concentrations in HSO_3Cl: (a) CVD CNTs at 5 ppm, (b) HiPco 188.3 at 10 ppm, (c) CCNI 1001 at 10 ppm, (d) CCNI 1002 at 10 ppm, (e) purified biochar at 10 ppm, and (f) nonpurified biochar at 10 ppm.

Table 1. Dataset Size (N Images), Number of Zero-End Point Images (N_p), Bootstrap Dataset Size (n), Average Length Estimate ($\langle L \rangle$), Average Bootstrap Length Estimate ($\langle L_{boot} \rangle$), and Standard Error of Estimate ($se_{\langle L \rangle}$ for Different Types of CNTs Computed from $N_{boot} = 10^6$ Bootstrapped Sets[a]

CNT source	$N = n$	N_p	$\langle L \rangle$ (μm)	$\langle L_{boot} \rangle$ (μm)	$se_{\langle L \rangle}$ (%)
HiPco batch 188.2	60	15	2.75	2.77	12.5
CVD	25	1	2.13	2.15	14.1
CCNI 1001	38	12	7.97	8.21	14.7
CCNI 1002	19	4	12.45	12.70	16.1
CCNI 1101	45	12	9.95	9.92	11.1
purified biochar	25	10	4.59	4.72	14.9
nonpurified biochar	42	17	6.87	7.11	18.5

[a]The size of all bootstrapped datasets was chosen to be the same as the total number of images in a dataset.

$(N_p/N)^n$ were non-negligible and the condition of eq 6 were not fulfilled. The inset of Figure 5 shows that the CVD dataset

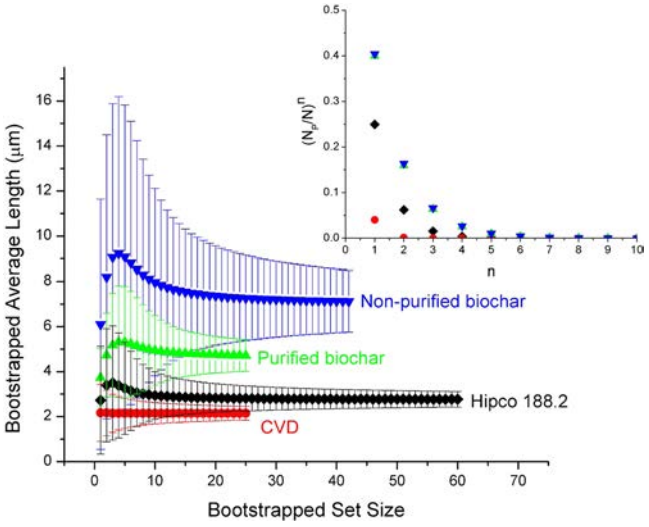

Figure 5. Bootstrapped length estimate and standard error as a function of bootstrap set size n for CVD, HiPco, purified biochar, and nonpurified biochar datasets. Inset shows probability of picking only images with zero end points as a function of n for each dataset. The legends for the plot and inset are the same.

has a small value of $(N_p/N)^n$, even for $n = 1$; thus, it is well-behaved because the bootstrapped length estimate is independent of n. All other datasets exhibit a maximum at low n before asymptotically decreasing toward a limit value because, at small n, the omission of bootstrapped sets consisting only of zero end point images induces a non-negligible bias toward shorter length estimates. As n grows, the probability of selecting only zero end point images becomes negligible, and these images' contribution to the length estimate is properly accounted. The inset plot of Figure 5 shows that, in the CVD dataset, the probability of choosing only zero end point images is negligible at $n = 1$ (<0.05). However, in the other datasets, this probability falls below 0.05 when $n > n_c \approx 3-4$, which coincides with the maximum in the plot of the bootstrapped length estimate. For instance, the non-purified and purified biochar datasets reach $(N_p/N)^n < 0.05$ when $n_c = 3$, in the HiPco, CCNI 1001, CCNI 1002, and CCNI 1101 datasets, whereas this criterion is met when $n_c = 4$ for the purified and nonpurified biochar datasets (see Figures 5 and 6).

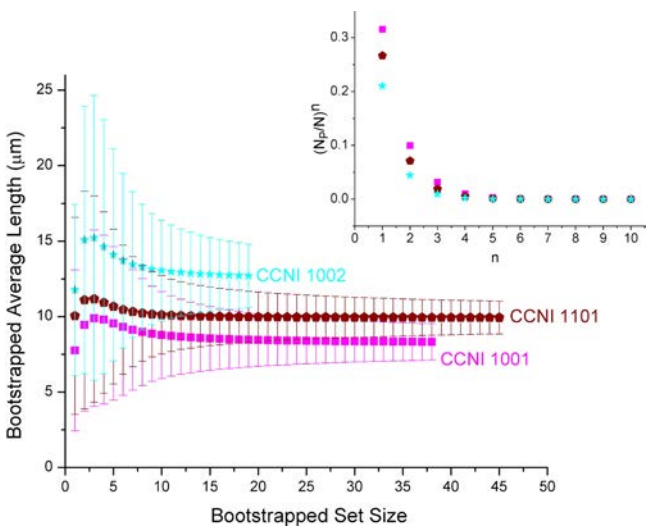

Figure 6. Bootstrapped length estimate and standard error as a function of bootstrap set size n for CCNI 1002, CCNI 1002, and CCNI 1101 datasets. Inset shows the probability of picking only images with zero end points as a function of n for each dataset. The legends for the plot and inset are the same.

We further check the behavior the standard errors in the range of validity of the bootstrap $(n - n_c > 0)$, and fit them to a power law. Figures 7 and 8 show that our standard errors show

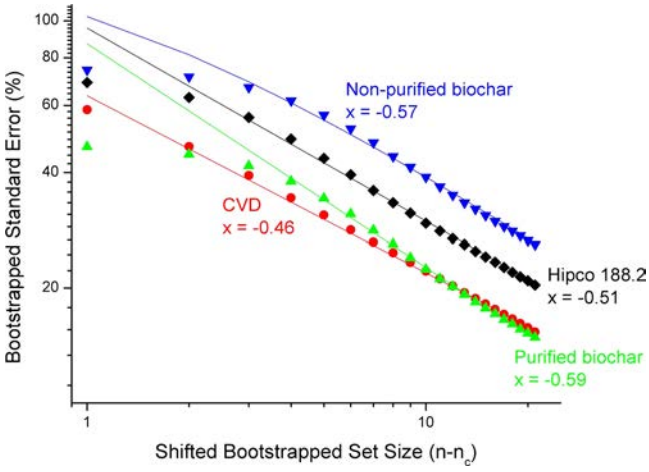

Figure 7. Bootstrapped standard error as a function of shifted bootstrap set size $(n - n_c)$ for the CVD, HiPco 188.3, purified biochar, and nonpurified biochar datasets with lines indicating corresponding power-law fits and exponents.

the expected asymptotic power law behavior with $x \approx -0.5$, indicating that they are a good estimate for the true variance of the CNT populations.

Relationship of CNT Length to Growth Method. The length measurement provides important insight into CNT production methods and the effect of CNT length on properties. HiPco batch 188.2 was produced by altering the reactor conditions by running at higher temperature (1030 °C instead of the standard 900 °C) at a catalyst flow rate approximately twice the standard (0.6 slm instead of the

dx.doi.org/10.1021/am500424u | ACS Appl. Mater. Interfaces 2014, 6, 6139−6146

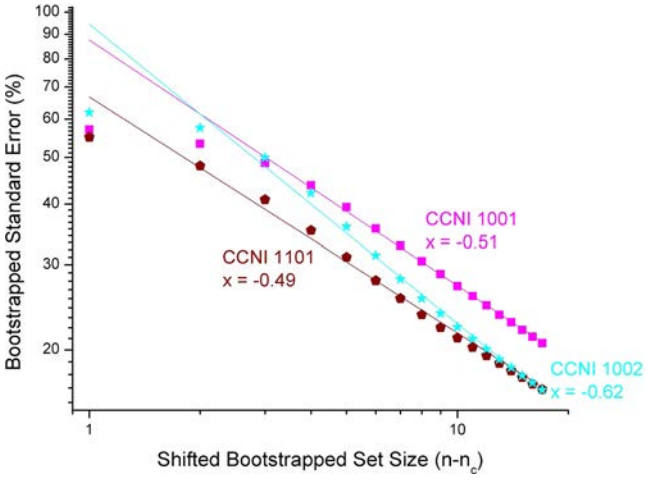

Figure 8. Bootstrapped standard error as a function of shifted bootstrap set size $(n - n_c)$ for the CCNI 1001, CCNI 1002, and CCNI 1101 datasets with lines indicating corresponding power-law fits and exponents.

standard 0.3 slm of iron-carrying gas stream). Previous shear rheology and AFM measurements[43] had shown that the viscosity-average length of HiPco batch 120.3, which had been produced under similar conditions (980 °C with 0.5 slm catalyst flow rate), was 950 nm. Since the viscosity-average length is always larger than the number-average length, our length estimate for the HiPco sample is ∼3 times higher than what was previously reported.

The length measurements provide insight on the properties of CNTs grown from a planar substrate. CVD CNTs were grown into a carpet configuration with a carpet height of ∼15 μm, as measured by taking a SEM image of the carpet.[31] However, our measurements yield a lower length (∼2.1 μm) for the individual CNTs constituting this carpet, supporting the literature view that individual CNTs do not grow continuously from the substrate to the top of the carpet and are shorter than the carpet height.[24]

CCNI CNTs were produced under different conditions for the purpose of studying the impact of CNT length on the properties of macroscopic materials.[13] Our results show that batches of CNTs with different lengths can be produced by tuning reactor conditions. The lengths of the CCNI samples measured by extensional rheology[32] were up to a factor of 3 less than the lengths measured here by cryo-TEM; this deviation is consistent with the over-estimation observed for the HiPco sample. The literature supports the view that the tensile strength of CNT fibers scales linearly with the CNT aspect ratio.[15] Previous work[32] has shown that fibers spun from the CCNI 1101 CNTs had a higher breaking force than the fibers spun from the CCNI 1001 CNTs, which is consistent with the length measurement results reported here. However, ref 32 reports that the CCNI 1002 CNTs yielded fibers with a lower breaking force than the CCNI 1101 CNTs (yet still larger than the CCNI 1001 CNTs)—this may be due to structural imperfections in the fibers spun out of the CCNI 1002 batch, or may simply be related to the fact that our length estimate of batches 1002 and 1101 are within ∼20% of each other, almost within the standard error of the measurement.

The biochar SWNTs were produced using a laser ablation method[34,35] on a novel biochar target and were thought to be longer than SWNTs previously synthesized using graphitic targets.[33] Our measurements show that the raw biochar SWNTs have an average length of ∼6.9 μm, which is high for laser ablation SWNTs (which are typically <0.5 μm),[44] even though there have been reports of individual laser ablation SWNTs above 10 μm in length.[45] Purification reduces the length to ∼4.6 μm, which is still longer than the typical length of high-quality laser ablation SWNTs, which explains the better performance of biochar SWNTs in polymer composites.[34]

Application of Statistical Method to AFM. For comparison with length measurement results of short CNTs that were measured individually, the method is also applied to five AFM height images.[42] The lengths and ends are measured and counted by the user-guided MATLAB program mentioned in the Experimental Methods section. A typical AFM height image and image analysis result are shown in Figure 9. Once the image analysis result is deemed satisfactory, each AFM image was segmented into nine smaller sub-images to increase the resolution of the bootstrap analysis.

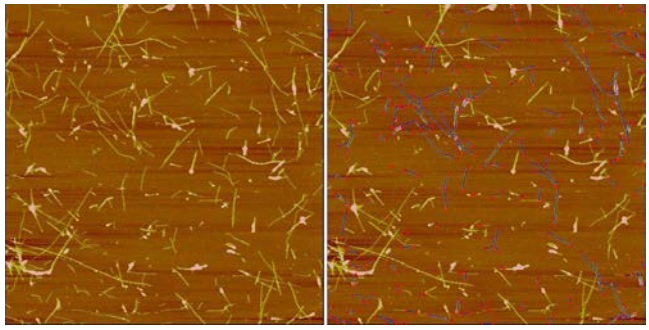

Figure 9. (left) AFM height micrograph of HiPco CNTs dispersed in DNA and (right) corresponding length and end point detection result. Detected CNTs are shown in blue and detected CNT end points are marked by red plus sign (+) symbols. The height data (shown in false color) indicates that the remaining structures are CNT bundles. The width of an individual AFM image is 10 microns.

Figure 9 clearly shows that not all CNTs are included in the analysis. The MATLAB code uses the height data in the AFM image to avoid measuring bundles of CNTs, which could potentially hide CNT end points, thus biasing the measurement toward a longer length estimate. Given the multitude of CNTs in each image, even after image segmentation the HiPco AFM dataset had no problematic zero end point images, and so we did not have to shift the standard error plot to observe its expected behavior (Figure 10).

Figure 9 shows that our analysis of the five AFM images produced a length average estimate of 216 nm, which is in excellent agreement with the authors' reported average length of 232 nm obtained from individual length measurements.[42] In addition, Figure 10 indicates that the standard error also has the expected behavior, with a power-law factor of $x = -0.51$.

CONCLUSIONS

In this study, the bootstrap method was applied to cryo-TEM and AFM images of CNTs to obtain average length estimates from direct measurements. The cryo-TEM method of analyzing CNTs in HSO_3Cl has the particular advantage of requiring no sonication during the sample preparation process, eliminating a frequent source of bias in CNT length measurement methods. Cryo-TEM is also insensitive to the presence of impurities, such as graphitic particles (as often encountered in laser-ablation

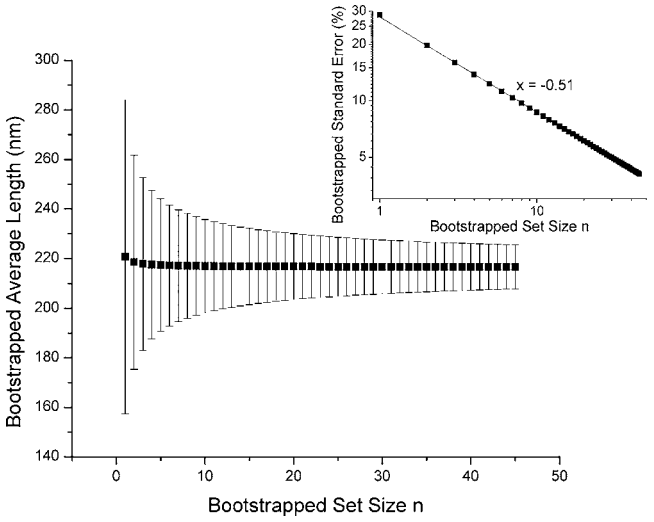

Figure 10. Bootstrapped length estimate and standard error as a function of bootstrapped set size *n* for the HiPco AFM dataset.

SWNTs), and, hence, is well-suited to examine raw samples before purification (which may affect length). Yet, cryo-TEM imaging appears to bias the length estimate towards longer CNTs, likely because shorter CNTs are difficult to identify through imaging. Another drawback—the time-expensive nature of direct imaging methods to obtain CNT length measurements (common to both cryo-TEM and AFM)—is overcome by the statistical efficiency of the bootstrap method, which has been shown to yield accurate results from relatively few images of CNTs.

AUTHOR INFORMATION

Corresponding Author

*E-mail: mp@rice.edu.

Notes

The authors declare no competing financial interest.

ACKNOWLEDGMENTS

We thank the following individuals: Yachin Cohen, for useful discussions; William Meddaugh, for advice and discussion about the bootstrap method; Nicholas Parra-Vasquez and Juan Duque, for providing the AFM images; Cary Pint and Bob Hauge, for providing the CVD SWNTs; Benoit Simard, Chris Kingston, and Jingwen Guan, for providing bio-laser SWNTs; Ed Vega, Xiaodong Xu, and Ken McElrath, for providing CCNI CNTs; and Steven Ho and Chris Harris, for providing HiPco SWNTs. This work was supported by the U.S.−Israel Binational Science Foundation (Grant No. 2012223), the Welch Foundation (Grant No. C-1668), the U.S. Air Force Office of Scientific Research (Grant No. FA9550-09-1-0590), and MURI (Grant No. FA9550-12-1-0035). Support from Teijin Aramid BV, Teijin Techno Products, Ltd., the Russell Berrie Nanotechnology Institute, and a gift by the H. Rich family are also acknowledged. The cryo-TEM work was performed at the Technion Laboratory for Electron Microscopy of Soft Matter, a Technion Russell Berrie Nanotechnology Institute (RBNI) infrastructure facility.

REFERENCES

(1) Huang, S.; Cai, X.; Liu, J. Growth of Millimeter-Long and Horizontally Aligned Single-Walled Carbon Nanotubes on Flat Substrates. *J. Am. Chem. Soc.* **2003**, *125*, 5636−5637.

(2) Yu, M.-F.; Files, B. S.; Arepalli, S.; Ruoff, R. S. Tensile Loading of Ropes of Single Wall Carbon Nanotubes and their Mechanical Properties. *Phys. Rev. Lett.* **2000**, *84*, 5552−5555.

(3) Che, J.; Cagin, T.; Goddard, W. A., III. Thermal Conductivity of Carbon Nanotubes. *Nanotechnology* **2000**, *11*, 65−69.

(4) Ebbesen, T. W.; Lezec, H. J.; Hiura, H.; Bennett, J. W.; Ghaemi, H. F.; Thio, T. Electrical Conductivity of Individual Carbon Nanotubes. *Nature* **1996**, *382*, 54−56.

(5) Baughman, R. H.; Zakhidov, A. A.; de Heer, W. A. Carbon Nanotubes—The Route Toward Applications. *Science* **2002**, *297*, 787−792.

(6) Bose, S.; Khare, R. A.; Moldenaers, P. Assessing the Strengths and Weaknesses of Various Types of Pre-Treatments of Carbon Nanotubes on the Properties of Polymer/Carbon Nanotubes Composites: A Critical Review. *Polymer* **2000**, *51*, 975−993.

(7) Hilding, J.; Grulke, E. A.; Zhang, Z. G.; Lockwood, F. Dispersion of Carbon Nanotubes in Liquids. *J. Dispersion Sci. Technol.* **2003**, *24*, 1−41.

(8) Ramesh, S.; Ericson, L. M.; Davis, V. A.; Saini, R. K.; Kittrell, C.; Pasquali, M.; Billups, W. E.; Adams, W. W.; Hauge, R. H.; Smalley, R. E. Dissolution of Pristine Single Walled Carbon Nanotubes in Superacids by Direct Protonation. *J. Phys. Chem. B* **2004**, *108*, 8794−8798.

(9) Davis, V. A.; Parra-Vasquez, A. N. G.; Green, M. J.; Rai, P. K.; Behabtu, N.; Prieto, V.; Booker, R. D.; Schmidt, J.; Kesselman, E.; Zhou, W.; Fan, H.; Adams, W. W.; Hauge, R. H.; Fischer, J. E.; Cohen, Y.; Talmon, Y.; Smalley, R. E.; Pasquali, M. True Solutions of Single-Walled Carbon Nanotubes for Assembly into Macroscopic Materials. *Nat. Nanotechnol.* **2009**, *4*, 830−834.

(10) Ericson, L. M.; Fan, H.; Peng, H.; Davis, V. A.; Zhou, W.; Sulpizio, J.; Wang, Y.; Booker, R.; Vavro, J.; Guthy, C.; Parra-Vasquez, A. N. G.; Kim, M. J.; Ramesh, S.; Saini, R. K.; Kittrell, C.; Lavin, G.; Schmidt, H.; Adams, W. W.; Billups, W. E.; Pasquali, M.; Hwang, W.-F.; Hauge, R. H.; Fischer, J. E.; Smalley, R. E. Macroscopic, Neat, Single-Walled Carbon Nanotube Fibers. *Science* **2004**, *305*, 1447−1449.

(11) Davis, V. A.; Ericson, L. M.; Parra-Vasquez, A. N. G.; Fan, H.; Wang, Y. H.; Prieto, V.; Longoria, J. A.; Ramesh, S.; Saini, R. K.; Kittrell, C.; Billups, W. E.; Adams, W. W.; Hauge, R. H.; Smalley, R. E.; Pasquali, M. Phase Behavior and Rheology of SWNTs in Superacids. *Macromolecules* **2004**, *37*, 154−160.

(12) Zhou, W.; Fischer, J. E.; Heiney, P. A.; Fan, H.; Davis, V. A.; Pasquali, M.; Smalley, R. E. Single-Walled Carbon Nanotubes in Superacid: X-ray and Calorimetric Evidence for Partly Ordered H_2SO_4. *Phys. Rev. B* **2005**, *72*, 045440.

(13) Behabtu, N.; Young, C. C.; Tsentalovich, D. E.; Kleinerman, O.; Wang, X.; Ma, A. W. K.; Bengio, E. A.; ter Waarbeek, R. F.; de Jong, J. J.; Hoogerwerf, R. E.; Fairchild, S. B.; Ferguson, J. B.; Maruyama, B.; Kono, J.; Talmon, Y.; Cohen, Y.; Otto, M. J.; Pasquali, M. Strong, Light, Multifunctional Fibers of Carbon Nanotubes with Ultrahigh Conductivity. *Science* **2013**, *339*, 182−186.

(14) Mirri, F.; Ma, A. W. K.; Hsu, T. T.; Behabtu, N.; Eichmann, S. L.; Young, C. C.; Tsentalovich, D. E.; Pasquali, M. High-Performance Carbon Nanotube Transparent Conductive Films by Scalable Dip Coating. *ACS Nano* **2012**, *6*, 9737−9744.

(15) Yakobson, B. I.; Samsonidze, G.; Samsonidze, G. G. Atomistic Theory of Mechanical Relaxation in Fullerene Nanotubes. *Carbon* **2000**, *38*, 1675−1680.

(16) Zhang, X.; Li, Q.; Tu, Y.; Li, Y.; Coulter, J. Y.; Zheng, L.; Zhao, Y.; Jia, Q.; Peterson, D. E.; Zhu, Y. Strong Carbon-Nanotube Fibers Spun from Long Carbon-Nanotube Arrays. *Small* **2007**, *3*, 244−248.

(17) Fagan, J. A.; Bauer, B. J.; Hobbie, E. K.; Becker, M. L.; Hight Walker, A. R.; Simpson, J. R.; Chun, J.; Obrzut, J.; Baipai, V.; Phelan, F. R.; Simien, D.; Huh, J. Y.; Migler, K. B. Carbon Nanotubes: Measuring Dispersion and Length. *Adv. Mater.* **2011**, *23*, 338−348.

(18) Islam, M. F.; Rojas, E.; Bergey, D. M.; Johnson, A. T.; Yodh, A. G. High Weight Fraction Surfactant Solubilization of Single-Wall Carbon Nanotubes in Water. *Nano Lett.* **2003**, *3*, 269−273.
(19) Wang, S.; Liang, Z.; Wang, B.; Zhang, C. Statistical Characterization of Single-Wall Carbon Nanotube Length Distribution. *Nanotechnology* **2006**, *17*, 634−639.
(20) Badaire, S.; Poulin, P.; Maugey, M.; Zakri, C. In Situ Measurements of Nanotube Dimensions in Suspensions by Depolarized Dynamic Light Scattering. *Langmuir* **2004**, *20*, 10367−10370.
(21) Hennrich, F.; Krupke, R.; Arnold, K.; Stütz, J. A. R.; Lebedkin, S.; Koch, T.; Schimmel, T.; Kappes, M. M. The Mechanism of Cavitation-Induced Scission of Single-Walled Carbon Nanotubes. *J. Phys. Chem. B* **2007**, *111*, 1932−1937.
(22) Pagani, G.; Green, M. J.; Poulin, P.; Pasquali, M. Competing Mechanisms and Scaling Laws for Carbon Nanotube Scission by Ultrasonication. *Proc. Natl. Acad. Sci. U.S.A.* **2012**, *109*, 11599−11604.
(23) Lucas, A.; Zakri, C.; Maugey, M.; Pasquali, M.; van der Schoot, P.; Poulin, P. Kinetics of Nanotube and Microfiber Scission under Sonication. *J. Phys. Chem. C* **2009**, *113*, 20599−20605.
(24) Jackson, J. J.; Puretzky, A. A.; More, K. L.; Rouleau, C. M.; Eres, G.; Geohegan, D. B. Pulsed Growth of Vertically Aligned Nanotube Arrays with Variable Density. *ACS Nano* **2010**, *4*, 7573−7581.
(25) Casey, J. P.; Bachilo, S. M.; Moran, C. H.; Weisman, R. B. Chirality-Resolved Length Analysis of Single-Walled Carbon Nanotube Samples through Shear-Aligned Photoluminescence Anisotropy. *ACS Nano* **2008**, *2*, 1738−1746.
(26) Parra-Vasquez, A. N. G.; Stepanek, I.; Davis, V. A.; Moore, V. C.; Haroz, E. H.; Shaver, J.; Hauge, R. H.; Smalley, R. E.; Pasquali, M. Simple Length Determination of Single-Walled Carbon Nanotubes by Viscosity Measurements in Dilute Suspensions. *Macromolecules* **2007**, *40*, 4043−4047.
(27) Khripin, C. Y.; Arnold-Medabalimi, N.; Zheng, M. Molecular-Crowding-Induced Clustering of DNA-Wrapped Carbon Nanotubes for Facile Length Fractionation. *ACS Nano* **2011**, *5*, 8258−8266.
(28) Parra-Vasquez, A. N. G.; Behabtu, N.; Green, M. J.; Pint, C. L.; Young, C. C.; Schmidt, J.; Desselman, E.; Goyal, A.; Ajayan, P. M.; Cohen, Y.; Talmon, Y.; Hauge, R. H.; Pasquali, M. Spontaneous Dissolution of Ultralong Single- and Multiwalled Carbon Nanotubes. *ACS Nano* **2010**, *4*, 3969−3978.
(29) Behabtu, N.; Lomeda, J. R.; Green, M. J.; Higginbotham, A. L.; Sinitskii, A.; Kosynkin, D. V.; Tsentalovich, D.; Parra-Vasquez, A. N. G.; Schmidt, J.; Kesselman, E.; Cohen, Y.; Talmon, Y.; Tour, J. M.; Pasquali, M. Spontaneous High-Concentration Dispersions and Liquid Crystals of Graphene. *Nat. Nanotechnol.* **2010**, *5*, 406−411.
(30) Bronikowski, M. J.; Willis, P. A.; Colbert, D. T.; Smith, K. A.; Smalley, R. E. Gas-Phase Production of Carbon Single-Walled Nanotubes from Carbon Monoxide via the HiPco Process: A Parametric Study. *J. Vac. Sci. Technol.* **2001**, *19*, 1800−1805.
(31) Amama, P. B.; Pint, C. L.; Mirri, F.; Pasquali, M.; Hauge, R. H.; Maruyama, B. Catalyst-Support Interactions and their Influence in Water-Assisted Carbon Nanotube Carpet Growth. *Carbon* **2012**, *50*, 2396−2406.
(32) Behabtu N. *Dissolution, Processing and Fluid Structure of Graphene and Carbon Nanotube in Superacids: The Route Toward High Performance Multifunctional Materials*. Ph.D. Thesis, Rice University, Houston, TX, 2012.
(33) Kingston, C. T.; Jakubek, Z. J.; Denommee, S.; Simard, B. Efficient Laser Synthesis of Single-Walled Carbon Nanotubes Through Laser Heating of the Condensing Vaporization Plume. *Carbon* **2004**, *42*, 1657−1664.
(34) Fraser, R. A.; Stoeffler, K.; Ashrafi, B.; Zhang, Y. F.; Simard, B. Large-Scale Production of PMMA/SWCNT Composites Based on SWCNT Modified with PMMA. *ACS Appl. Mater. Interfaces* **2012**, *4*, 1990−1997.
(35) Kingston, C. T. Highly Efficient Laser Synthesis of SWCNT from Renewable Carbon, and Process Development for Large Scale Synthesis of SWCNT by RF Induction Thermal Plasma. Presented at *Guadalupe Workshop*, April 2011.
(36) Bellare, J. R.; Davis, H. T.; Scriven, L. E.; Talmon, Y. Controlled Environment Vitrification System—An Improved Sample Preparation Technique. *J. Electron Microsc.* **1988**, *10*, 87−111.
(37) Fagan, J. A.; Landi, B. J.; Mandelbaum, I.; Simpson, J. R.; Bajpai, V.; Bauer, B. J.; Migler, K.; Hight Walker, A. R.; Raffaelle, R.; Hobbie, E. K. Comparative Measures of Single-Wall Carbon Nanotube Dispersion. *J. Phys. Chem. B* **2006**, *110*, 23801−23805.
(38) Ziegler, K. J.; Rauwald, U.; Gu, Z. N.; Liang, F.; Billups, W. E.; Hauge, R. H.; Smalley, R. E. Statistically Accurate Length Measurements of Single-Walled Carbon Nanotubes. *J. Nanosci. Nanotechnol.* **2007**, *7*, 2917−2921.
(39) Efron, B. Boostrap Methods: Another Look at the Jacknife. *Ann. Stat.* **1979**, *7*, 1−26.
(40) Green, M. J.; Parra-Vasquez, A. N. G.; Behabtu, N.; Pasquali, M. Modeling the Phase Behavior of Polydisperse Rigid Rods with Attractive Interactions with Applications to Single-Walled Carbon Nanotubes in Superacids. *J. Chem. Phys.* **2009**, *131*, 084901.
(41) Kleinerman, O.; Parra-Vasquez, A. N. G.; Green, M. J.; Behabtu, N.; Schmidt, J.; Kesselman, E.; Young, C. C.; Cohen, Y.; Pasquali, M.; Talmon, Y. Cryogenic-Temperature Electron Microscopy for Direct Imaging of Carbon Nanotubes and Graphene Dissolved in Superacids. Manuscript in preparation.
(42) Parra-Vasquez, A. N. G.; Duque, J. G.; Green, M. J.; Pasquali, M. Assessment of Length and Bundle Distribution of Dilute Single-Walled Carbon Nanotubes by Viscosity Measurements. *AIChE J.* **2014**, *60*, 1499−1508 (DOI: 10.1002/aic.14325).
(43) Parra-Vasquez, A. N. G. *Solubility, Length Characterization, and Cryo-TEM of Pristine and Functionalized Single-Walled Carbon Nanotubes in Surfactant and Superacid Systems, with Application to Spinning SWNT Fibers*. Ph.D. Thesis, Rice University, Houston, TX, 2009.
(44) Puretzky, A. A.; Schittenhelm, H.; Fan, X.; Lance, M. J.; Allard, L. F., Jr.; Geohegan, D. B. Investigations of Single-Wall Carbon Nanotube Growth by Time-Restricted Laser Vaporization. *Phys. Rev. B* **2002**, *65*, 245425.
(45) Puretzky, A. A.; Geohegan, D. B.; Fan, X.; Pennycook, S. J. In Situ Imaging and Spectroscopy of Single-Wall Carbon Nanotube Synthesis by Laser Vaporization. *Appl. Phys. Lett.* **2000**, *76*, 182.